JOURNAL OF THERMOPHYSICS AND HEAT TRANSFER
Vol. 23, No. 2, April–June 2009

Rib-Spacing Effect on Heat Transfer in Rectangular Channels at High Rotation Numbers

Michael Huh,* Yao-Hsein Liu,* and Je-Chin Han†
Texas A&M University, College Station, Texas 77843
and
Sanjay Chopra‡
Siemens Power Company, Orlando, Florida 32826

DOI: 10.2514/1.37512

This study experimentally determined the effects of rib spacing on heat transfer in a rotating 1:4 AR channel with a sharp-bend entrance. The leading and trailing walls used 45 deg angled ribs. The rib-height-to-hydraulic-diam ratio e/D_h was 0.078. The rib-pitch-to-rib-height ratios P/e studied were $P/e = 2.5$, 5, and 10. Each ratio was tested at five Reynolds numbers up to 40,000. For each Reynolds number, experiments were conducted at five rotational speeds up to 400 rpm. Results showed that the sharp-bend entrance has a significant effect on the first-pass heat transfer enhancement. In the second pass, the rib spacing and rotation effect are reduced. The $P/e = 10$ case had the highest heat transfer enhancement, based on the total area, and the $P/e = 2.5$ had the highest heat transfer enhancement, based on the projected area. The current study has extended the range of the rotation number Ro and local buoyancy parameter Bo_x for a ribbed 1:4 AR channel up to 0.65 and 1.5, respectively. Correlations for predicting heat transfer enhancement due to rotation in the ribbed 1:4 AR channel, based on the extended range of the rotation number and buoyancy parameter, are presented in the paper.

Nomenclature

AR	=	channel aspect ratio, W:H
A_h	=	total heater surface area, mm^2
A_p	=	projected surface area, mm^2
A_t	=	total heat transfer surface area for the segment, mm^2
Bo_x	=	local buoyancy parameter
c_p	=	specific heat at constant pressure, J/kg · K
D_h	=	channel hydraulic diameter, m^2
e	=	rib height, mm
H	=	channel height, mm
h	=	regionally averaged heat transfer coefficient, W/m^2 · K
I	=	current, A
i	=	given region in the channel ($1 \leq i \leq 12$)
k	=	thermal conductivity of the coolant, W/mK
L	=	length of the heated portion of the test section, mm
m	=	mass flow rate, kg/s
Nu	=	regionally averaged Nusselt number
Nu_o	=	Nusselt number for fully developed turbulent flow in a nonrotating smooth pipe
Nu_s	=	stationary regionally averaged Nusselt number
P	=	rib pitch, mm
Pr	=	Prandtl number of the coolant
Q_{loss}	=	external heat loss, W
Q_{net}	=	net heat transfer, W
R	=	mean radius of rotation, mm
Re	=	Reynolds number
Ro	=	rotation number
R_x	=	local radius of rotation, mm
$T_{b,\text{in}}$	=	bulk fluid temperature at the inlet of a given region, °C or K
$T_{b,\text{out}}$	=	bulk fluid temperature at the outlet of a given region, °C or K
$T_{b,x}$	=	local coolant bulk temperature, °C or K
$T_{f,x}$	=	local film temperature, °C or K
$T_{w,x}$	=	regionally averaged wall temperature, °C or K
U_b	=	bulk velocity in the streamwise direction, m/s
V	=	voltage, V
W	=	channel width, mm
β	=	angle of channel orientation with respect to the axis of rotation, deg
$\Delta\rho$	=	local bulk-wall density difference ($\rho_{b,x}$–$\rho_{w,x}$)
μ	=	viscosity of the coolant, Pa · s
$\rho_{b,x}$	=	local density of air based on local bulk air temperature, kg/m^3
$\rho_{w,x}$	=	local density of air based on local wall temperature, kg/m^3
Ω	=	rotational speed, rad/s

Introduction

THE applications for gas turbines range from land-based power generation to aircraft engines (commercial and military) to the oil and gas industries. Clearly, the efficiency and power production of gas turbines has a large impact in many different areas. Much research has been initiated and conducted by industry, government agencies, and universities over the past several decades to improve the design of gas turbines with respect to heat transfer. The ability to increase the turbine inlet temperatures, which in turn increases efficiency and power, is partially due to the turbine blade cooling techniques developed through research. One such heat transfer enhancement technique is the inclusion of rib turbulators (trip strips) on the internal walls of the pressure and suction surfaces of the gas turbine blade, as shown in Fig. 1. From this figure, it is seen that internal channels are manufactured in the gas turbine blade. As hot gases from the combustor pass over the blade, heat is transferred from the hot gases to the blade external surface and is then conducted through the blade wall. In the internal passages, cool air bled from the compressor stage is circulated to remove heat from the blade surface. Thus, high heat transfer on the walls of internal cooling passages is desirable. If insufficient heat is removed, the blade will be thermally

Received 12 March 2008; revision received 5 January 2009; accepted for publication 31 January 2009.

*Research Assistant, Department of Mechanical Engineering, Mail Stop 3123 TAMU.
†Distinguished Professor, Department of Mechanical Engineering, Mail Stop 3123 TAMU.
‡Manager, 4400 Alafaya Trail.

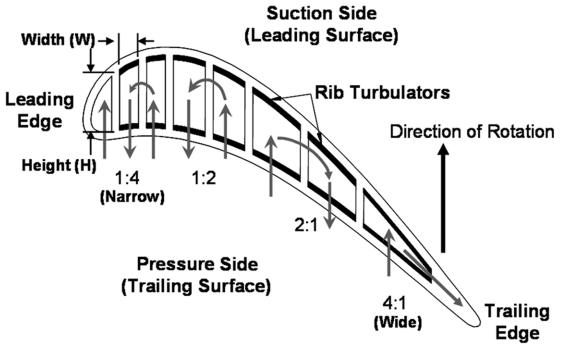

Fig. 1 Gas turbine blade internal cooling channels and their applicable aspect ratios.

stressed and could fracture. In general, as a fluid flows through a channel, a hydrodynamic and thermal boundary layer forms. It is well known that the formation of the boundary layer causes heat transfer to decrease as the fluid reaches a fully developed condition. By breaking the boundary layer and increasing turbulence, heat transfer can be increased. The rib turbulators in the gas turbine blade cooling channels serve this purpose.

In Fig. 1, it is also seen that the geometry of the internal channels varies from the leading edge to the trailing edge. Typically, in a laboratory experiment, a square or rectangular channel is used to model the internal cooling channels of a gas turbine blade. Depending upon the location of the internal channel, the channel may have a wide aspect ratio (i.e., suction and pressure surfaces are separated by a short distance), as is the case near the trailing-edge region. Rectangular channels with AR = 4:1 are used to model these channels. In the midportion of the blade, the internal channel is more square, and thus channels with AR = 2:1, 1:1, and 1:2 are used to model this region of the gas turbine blade internal cooling passage. Finally, near the leading edge of the blade, the internal channel has a narrow aspect ratio (i.e., suction and pressure surfaces are separated by a large distance). Rectangular channels with AR = 1:4 are used to simulate these channels.

Aspect Ratio Effects in Ribbed Channels (Stationary)

It has been shown that the heat transfer and fluid flow characteristics are dependent on the channel aspect ratio. Several studies have been performed under stationary conditions to understand how heat transfer varies in the different aspect ratio channels with smooth and ribbed walls. Han [1] studied the effect of the channel aspect ratio on heat transfer for five different channel aspect ratios (AR = 1:4, 1:2, 1:1, 2:1, and 4:1). The channels had ratios of rib pitch P to rib height e of $P/e = 10$ and 20. He concluded that the local heat transfer enhancement on the ribbed wall decreases with increasing P/e and that the local heat transfer in the narrow-aspect-ratio channel is higher than the wide-aspect-ratio channel. Han and Park [2] studied the combined effects of rib angle and channel aspect ratio in rib-roughened rectangular channels with AR = 1:1, 2:1, and 4:1 and with $P/e = 10$ and 20. They concluded that the heat transfer performance in the square channel with angled ribs is 30% higher than in the traverse-rib case. For AR = 2:1 and 4:1, the heat transfer performance with angled ribs is 5% higher than with traverse ribs. Park et al. [3] studied heat transfer and pressure drop in five different aspect ratio channels (AR = 1:4, 1:2, 1:1, 2:1, and 4:1) with different rib angles of 90, 60, 45, and 30 deg. All cases considered ribs with $P/e = 10$. The results showed that narrow-aspect-ratio channels have better heat transfer performance than wide-aspect-ratio channels. For the square channel and the narrow-aspect-ratio channels, the ribs with a 60 deg /45 deg rib angle have higher heat transfer performance. The wide-aspect-ratio channels give the best heat transfer performance with ribs at angles of 45 deg /30 deg.

Rib Pitch Effect (Stationary)

The rib spacing in the internal cooling passage is important. Placing too many ribs on the heat transfer surface could result in an increase in pressure drop. Not having enough ribs can result in minimal heat transfer due to minimal breaking of the boundary layer. To obtain the optimal rib spacing, the heat transfer enhancement and the pressure drop are both taken into account. Taslim and Spring [4] used a liquid crystal technique to investigate the effects of rib profile, rib spacing, and blockage ratios e/D_h on heat transfer and friction. From their experiments, they found that there is an optimum P/e for a given blockage ratio. Han et al. [5] studied the effects of rib spacing in a wide-aspect-ratio channel of 12:1. They measured heat transfer and pressure drop for $P/e = 5$, 7.5, 10, 15, and 20. Their results showed that for orthogonal ribs, the best heat transfer performance occurred for $P/e = 10$. Han [6] investigated rib spacing in a square channel with $P/e = 10$, 20, and 40. He showed that the average friction factor and Stanton number decreased with increasing P/e.

Rotation Number Effect

One drawback to the stationary experiments is that the effects of the Coriolis and rotation-induced buoyancy forces that occur under rotating conditions in a heated channel are not present. The flowfield is strongly affected by rotation and thereby the heat transfer. Wagner et al. [7,8] performed experiments in a smooth-wall square channel with both radially outward and radially inward flow in a multipass model. The rotation number for their tests ranged from 0.0–0.48. Their results showed that an increase in the rotation number will cause the heat transfer to increase on the trailing surface and to decrease on the leading surface for a radially-outward-flow condition. For the radially-inward-flow case, the leading-surface heat transfer was not affected greatly. The trailing-surface heat transfer is strongly impacted by the flow direction. Taslim et al. [9] performed experimental heat transfer testing using a liquid crystal technique. They studied the rotation effects in rotating channels with ribbed walls with $P/e = 10$. The rotation number for their tests ranged from 0.0–0.3. They noted that as the rotation number increased, the heat transfer also increased on the trailing surface. On the leading surface, the heat transfer decreased with an increase in rotation number. Azad et al. [10] and Al-Hadhrami et al. [11] performed rotating experiments in a 2:1 ribbed channel ($P/e = 10$) with rotation numbers ranging from 0.0–0.21. The results from Azad et al. [10] and Al-Hadhrami et al. [11] confirmed the results of Wagner et al. [7,8] and Taslim et al. [9]. Fu et al. [12] performed experiments in ribbed channels with AR = 1:2 and 1:4. The rotation number in their study ranged from 0.0–0.3. They concluded that the heat transfer was strongly dependent on the buoyancy parameter on the first-pass leading wall with radially outward flow. This result is different from that for the channels with AR = 2:1 and 4:1, for which the buoyancy parameter has a weak impact on the leading wall in the first pass. Fu et al. [13] further investigated the effects of buoyancy in five different aspect ratio channels (AR = 1:4, 1:2, 1:1, 2:1, and 4:1) with ribs. Their results showed that the overall levels of heat transfer enhancement for all ribbed channels were comparable. However, the pressure drop was strongly dependent on the channel aspect ratio. Su et al. [14] performed a CFD study on rotating 45 deg angled ribbed channels with AR = 1:1, 1:2, and 1:4. The rotation number in their computations ranged from 0.0–0.28. They concluded that for large Reynolds numbers and rotation numbers, the effect of rotation decreases with a decrease in aspect ratio. Liu et al. [15] considered four different P/e ratios in a rotating 1:2 AR channel. The rotation number in their study ranged from 0.0–0.2. Their results showed that for their aspect ratio channel, the best heat transfer performance was for a close rib spacing of $P/e = 3$ based on projected surface area. The $P/e = 5$ case showed the greatest pressure drop. They also noted that the effect of rotation becomes stronger with smaller rib spacing.

Entrance Effects (Rotating)

Many of the studies have focused on rotating channels with a fully developed entrance condition. However, in a gas turbine blade, the

flow is in the developing state. It is well known that heat transfer behavior is different for fully developed flow when compared with flow in the entrance region. Wright et al. [16] performed experiments in channels with three different entrance geometries (fully developed flow, sudden contraction, and partial sudden contraction). They concluded that the entrance condition will enhance the heat transfer. They also pointed out that increasing the rotation number will decrease the effect of the entrance. The influence of the entrance geometry is also stronger in the smooth channel than in the ribbed channel. Wright et al. [17] and Liu et al. [18] extended the rotation number [$Ro = 1.0$ (Wright et al. [17]) and $Ro = 0.67$ (Liu et al. [18])] in a smooth-wall channel. Wright et al. [17] showed that the entrance contraction enhanced heat transfer near the entry region of the channel. Liu et al. [18] showed that the sharp-bend entrance condition reduced the effect of rotation in the first passage. In the second pass, the entrance geometry had little effect, due to the strong turn effect.

Objectives

Early research involving rib turbulators started in stationary channels. Most of the work at that time considered traverse ribs. Further work showed that if the ribs were placed at an angle, the heat transfer enhancement would increase, while simultaneously decreasing the pressure penalty. Experiments that considered the effects of rotation combined with ribs have mostly considered square and wide-aspect-ratio channels. However, it is clear that the aspect ratio, rib spacing, and rotation have an impact on the heat transfer distribution in the channel. Up to this point, only limited research has been presented for rotating channels with AR = 1:4 with ribbed walls. Fu et al. [12,13] presented data for a ribbed 1:4 channel, but the rotation number was limited to 0.3 and only one P/e ratio was presented. The entrance condition for their channel was fully developed. To model the 1:4 channel more like a gas turbine blade, Liu et al. [18] considered a sharp-bend entrance condition. They extended the rotation number for the 1:4 AR channel to 0.67. However, their study was for a smooth surface only. The current study aims to provide additional information for the 1:4 channel in terms of heat transfer with ribs at large rotation numbers and with a realistic entrance condition. The objectives of the current study are as follows:

1) Investigate the effects of rib-pitch-to-rib-height ratio P/e on the regionally averaged heat transfer coefficient in a two-pass 1:4 AR channel. To accomplish this task, three P/e ratios were considered: $P/e = 2.5$, 5, and 10. The angle of the ribs was held constant at 45 deg.

2) Determine the effects that rotation has on the rib-roughened leading and trailing surfaces in the first and second passes of the 1:4 AR channel.

3) Develop correlations to predict the heat transfer enhancement due to rotation on the rib-roughened walls of the 1:4 AR channel.

4) Extend the range of the rotation number and buoyancy parameter in the 1:4 AR channel with 45 deg rib-roughened walls. The target Ro and Bo parameters for the current study are 0.65 and 1.5, respectively. The current study Ro is more than twice that previously reported for the ribbed 1:4 AR channel.

5) Investigate the effects of the inlet geometry (sharp bend) on heat transfer with rib-roughened surfaces. A sharp-bend entrance that turns the flow 90 deg twice before entering the heated region of the test channel is used to create a developing flow region in the first pass.

Experimental Setup

Typical rotation numbers for aircraft engines are near 0.25 with Reynolds numbers in the range of 50,000. One method to achieve similar conditions for the large rotation number in the laboratory is to use air at high pressures. As the pressure of the air increases, so will the density. For a fixed mass flow rate (Reynolds number) and hydraulic diameter, an increase in density will result in a decrease in velocity. A lower velocity will in turn increase the rotation number. To achieve larger rotation numbers at higher Reynolds numbers, the experiments for the present study were conducted with air at a pressure of 75 psig. For the current study, a rotation number of 0.65 and 0.16 can be achieved at Reynolds numbers of 10,000 and 40,000, respectively.

Rotating Facility

Figure 2 shows the rotating arm assembly used to conduct the experiments for the current study. A steel table is used as the support structure. A 25 hp electric motor is used to drive the shaft, which in turn spins the arm. Counterweights located opposite of the test-section housing are used to balance the arm so that minimal vibrations are experienced during rotation. The air from the compressor enters an American Society of Mechanical Engineers square-edge orifice meter (not shown) in which the mass flow rate is measured. Air enters the rotating assembly at the bottom of the shaft via a rotary union. The air then passes through the hub and into the bore of the arm. A rubber hose is used to direct the flow from the arm to the test-section housing. After the air flows through the test section, it exits the housing. The hot exhaust air is then directed to the slip ring by means of a rubber hose. A $\frac{1}{2}$ in. copper tube, which passes through the bore of the slip ring, is used to direct the air to the top rotary union. Steel pipe is connected to the top rotary union and a valve is used to adjust the backpressure of the system.

Test Section (AR = 1:4)

The entrance geometry with a redirected sharp bend is shown in Fig. 3a. The air passes through a 9.525 mm inlet hose into the curved plenum region. After direct impingement on the plenum region, the flow is redirected into the 1:4 AR test section, as shown. A screen is placed before the first copper-plate region of the test section to help spread the flow at the entrance. The wire diameter of the screen is 0.015 mm. A nylon substrate with a low thermal conductivity is used to support the copper plates and heaters. Between each copper plate is a strip of insulation material that prevents conduction between copper plates and also helps to create a smooth surface between adjacent copper plates.

As the air passes through the test section, it is heated using prefabricated silicone rubber heaters that are placed beneath the copper plates, as shown in Fig. 3b. A total of 12 heaters are used for the outer, inner, leading, and trailing walls. An additional heater is used for the tip. Thermally conductive paste is used between the heaters and the copper plates to reduce contact resistance. Blind holes with a diameter of 1.59 mm are drilled 1.59 mm deep on the backside of each copper plate. Thermocouples are placed inside of the blind holes of the copper plates and are affixed to the copper plates using highly conductive epoxy. The minimum thickness of the divider wall is 5.60 mm. Figure 3c shows that each passage is divided into six regions. There are a total of 12 regions in the test section. The overall test-section length is 190.50 mm. The heated channel length of each passage is 154.50 mm and the plenum length is 19.05 mm. One thermocouple is placed at the inlet to measure the air temperature as it enters the test section. At the exit of the test section, two thermocouples are used to measure the air temperature. Temperature measurements are taken on all of the leading, trailing, and tip-cap

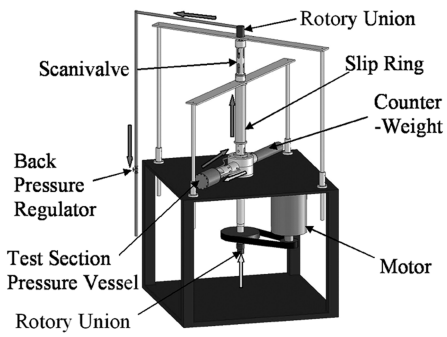

Fig. 2 Rotating arm assembly used to perform heat transfer experiments with the 1:4 AR test section.

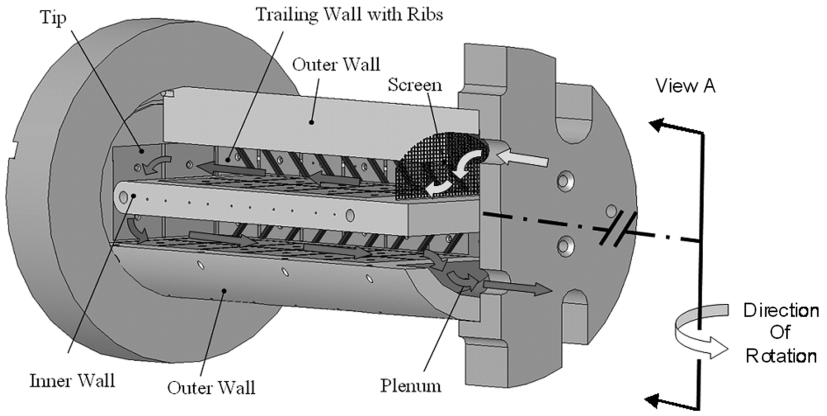

a)

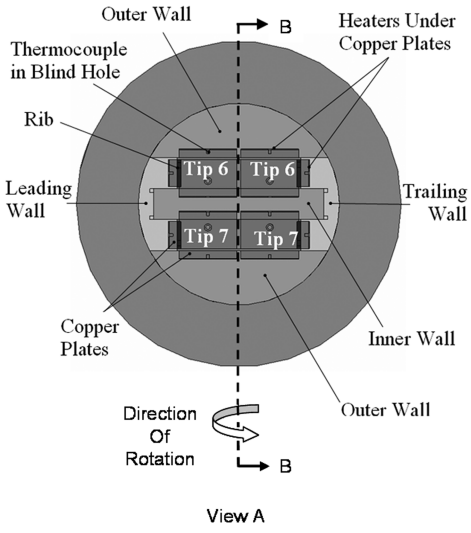

b)

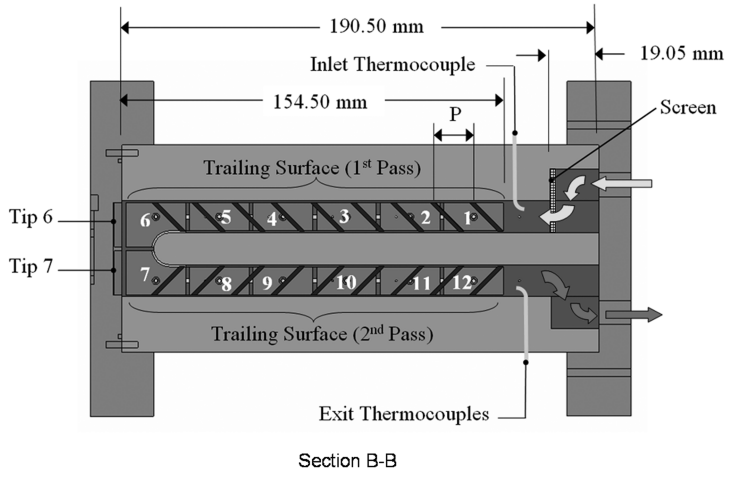

c)

Fig. 3 Illustrations of a) flow channel geometry of the 1:4 AR test section, b) test-section tip view showing location of heaters and wall naming convention, and c) test-section view showing the copper-plate region numbering convention.

copper plates. On the outer and inner walls, only the temperatures of the copper plates at regions four and ten are measured, due to limited slip-ring channels. The copper plates on the leading and trailing walls are rectangular in shape and measure 23.81×11.11 mm. The thickness of all copper plates is 3.175 mm. The outer and inner wall copper plates are square and measure 23.81×23.81 mm. The tip copper plates are rectangular with dimensions of 23.81×17.46 mm. The flow channel width is 50.8 mm and has a height of 12.70 mm, resulting in a hydraulic diameter D_h of 20.32 mm. The test section consists of two passes. The flow in the first passage is radially outward, and after a 180 deg turn, the flow is radially inward.

Figure 4 shows details of the rib-roughened surface of the test section. Ribs were placed on the leading and trailing walls of both passes in a parallel configuration. The ribs have a square cross section measuring 1.59×1.59 mm and are made of brass. The blockage ratio e/D_h is 0.078. A very thin layer of thermally conductive glue is used to affix the ribs to the surface of the copper plates. The ribs are placed at a 45 deg angle relative to the mainstream flow.

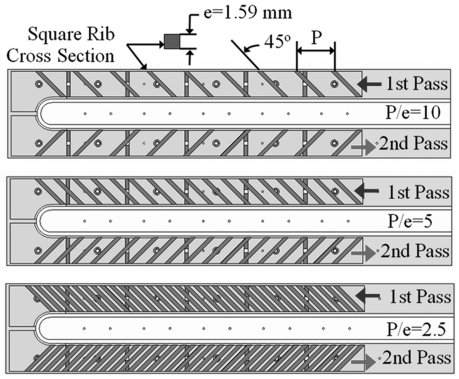

Fig. 4 Drawing showing the three different rib configurations tested.

For the present study, the test section is oriented 90 deg to the direction of rotation. Three different rib-pitch-to-rib-height P/e ratios are tested: $P/e = 2.5$, 5, and 10. The air pressure is maintained at 75 psig for all cases studied. For each P/e ratio, the Reynolds numbers tested are 10,000, 15,000, 20,000, 30,000, and 40,000. At each Reynolds number, the rotational speed is varied from 0 to 400 rpm with an increment of 100 rpm. The corresponding rotation number Ro and buoyancy parameter Bo at each Reynolds number and rotational speed tested are shown in Fig. 5.

Data Reduction

Heat Transfer Enhancement

This study investigates the regionally averaged heat transfer coefficient h at various locations within the rotating duct. A uniform wall temperature of 65°C in the circumferential direction is maintained at regions 4 and 10 throughout all of the tests. The density ratio is 0.11, based on the uniform wall temperature (65°C) and the temperature of the air at the inlet (23°C). In the current study, the regionally averaged heat transfer coefficient is calculated using the net heat transferred from the heated copper plate (Q_{net}), the total heat transfer surface area (A_t = smooth area between ribs, plus the area of 3 rib sides) at each region, the regionally averaged temperature of the plate ($T_{w,x}$), and the local bulk mean temperature of the airflow in the channel ($T_{b,x}$). Therefore, the regionally averaged heat transfer coefficient is given as

$$h = (Q_{\text{net}}/A_t)(T_{w,x} - T_{b,x}) \tag{1}$$

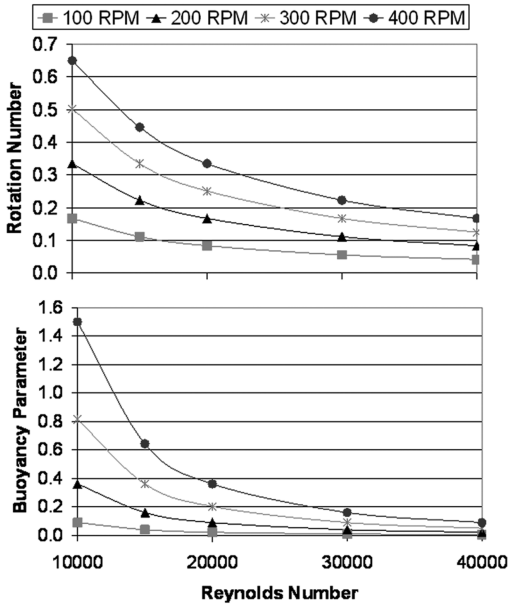

Fig. 5 Rotation number and buoyancy parameter at different Reynolds numbers and rotational speeds.

The net heat transfer is calculated as

$$Q_{\text{net}} = (V \cdot I)(A_p/A_h) - Q_{\text{loss}} \tag{2}$$

The voltage V is measured with a multimeter, and the current I is supplied to each heater by variac transformers. The power input to each heater is multiplied by the ratio of the projected heat transfer area A_p to the total heater area A_h. To determine the external heat losses Q_{loss} escaping from the test section during the experiment, two heat-loss calibration tests are performed. The first heat-loss calibration test is performed at a lower wall temperature than the experiment wall temperature. Similarly, a second heat-loss calibration test is performed at a higher wall temperature than the experiment wall temperature. During the heat-loss calibration tests, the wall temperature is maintained by supplying power to each heater with the variac transformers. A successful heat-loss calibration test is achieved when the total power input to the test section reaches equilibrium with the environment (i.e., the wall temperature reaches a constant value). The heat loss that occurs during the experiment is then determined by interpolating between the two sets of heat-loss data. It is noted that heat-loss calibration tests were performed at all rotational speed conditions considered in the present study and in the stationary case as well. To minimize natural convection effects during the heat-loss calibration tests, an insulating material was placed inside of the flow channels. The regionally averaged wall temperature $T_{w,x}$ is directly measured using the thermocouple installed in the blind hole on the backside of each copper plate. Because the plates are made of copper, which has a high thermal conductivity, the temperature of each plate is assumed to be uniform. One thermocouple at the inlet and two thermocouples at the outlet of the test section measure the inlet and outlet bulk temperatures, respectively. Therefore, the bulk temperature at any location in the test section can be calculated using linear interpolation. The results presented in this study are based on the linear interpolation method. Although linear interpolation was chosen for determining the coolant temperature at various locations in the channel, the bulk air temperature can also be calculated using the conservation of energy principle. For the present study, both methods compare very well. To determine the bulk air temperature by an energy balance, Eq. (3) can be used. Thus, for a given region i ($1 \le i \le 12$), the energy balance equation is

$$(T_{b,\text{out}} - T_{b,\text{in}})_i = \sum_i \frac{Q_{\text{net}}}{m \cdot c_p} \tag{3}$$

In Eq. (3), $T_{b,\text{in}}$ is the bulk air temperature at the inlet of region i, and $T_{b,\text{out}}$ is the bulk air temperature at the outlet of region i. The net heat transferred to the air from all four surfaces (leading, trailing, inner, and outer walls) at region i is divided by the product of the mass flow rate m and the specific heat c_p. Thus, for the first region at the channel inlet (region $i = 1$), $T_{b,\text{in}}$ is the actual measured temperature of the air using the channel inlet thermocouple. Heat is added to the air in region $i = 1$ from all four walls. This results in a bulk air temperature increase at the exit of region $i = 1$. At the exit of region $i = 1$, the bulk air temperature is $T_{b,\text{out}}$, which is also the inlet temperature for region $i = 2$. The local bulk air temperature $T_{b,x}$ in region i is then determined as the average of $T_{b,\text{in}}$ and $T_{b,\text{out}}$.

The Dittus-Boelter/McAdams correlation for heating ($T_{w,x} > T_{b,x}$) is used in this study to provide a basis of comparison. The Dittus-Boelter/McAdams correlation from Kays et al. [19] is used to calculate the Nusselt number Nu_o for fully developed turbulent flow through a smooth stationary pipe. Therefore, the regionally averaged Nu/Nu_o ratio is given as

$$(Nu/Nu_o) = \left(\frac{h \cdot D_h}{k}\right)\left(\frac{1}{0.023 \cdot Re^{0.8} \cdot Pr^{0.4}}\right) \tag{4}$$

where h is calculated by Eq. (1). All air properties taken are based on the channel average bulk air temperature with a Prandtl number Pr for air of 0.71.

Experimental Uncertainty

The uncertainty analysis performed is based on the method described by Kline and McClintock [20]. Air properties taken are based on the mean bulk air temperature. The estimated uncertainty for the temperature instrumentation is 0.5°C. The uncertainty of the Nu/Nu_o ratio is approximately 7% for the highest Reynolds number. For the lowest Reynolds number ($Re = 10,000$), the maximum uncertainty is approximately 10.2% on the low-heat-flux wall under rotating conditions.

Discussion of Results

Flowfield Behavior

Before discussing the experimental results for the two-pass 1:4 AR channel with angled ribs, it is necessary to understand the flow behavior inside the channel. The orientation of the rib turbulators has a significant impact on the level of heat transfer enhancement. Skewed ribs yield significantly higher heat transfer enhancement than orthogonal ribs. This is due to the additional secondary flow induced by the angle of the ribs. Rib turbulators are also widely known as "trip strips," as they simply trip the boundary layer in the internal channel. After the boundary layer is disturbed, redevelopment begins, and high heat transfer is associated with the thin boundary layer. Figure 6 presents conceptual views of the most notable characteristics of the effects of ribs on the mainstream flow. As shown in Fig. 6a, as the mainstream flow near the surface of the channel passes over the rib, it separates from the surface, due to the rib. This separation results in relatively low heat transfer just downstream of the rib, due to a relatively hot cell being trapped in the area of recirculation. However, when the mainstream flow reattaches to the surface (between two ribs), this is an area of relatively high heat transfer, due to impingement of the mainstream flow on the surface. This pattern of separation, recirculation, and reattachment continues throughout the channel, along with the pattern of repeating ribs. The ideal rib spacing is large enough for the mainstream flow to reattach to the surface between the ribs (high heat transfer), but not so large that the boundary layer is allowed to develop freely. By allowing the mainstream flow to develop freely, the advantage of the thin boundary layer is lost. In addition to general flow separation and reattachment, the rib turbulators increase turbulent mixing. The relatively hot fluid near the surface is continuously mixing with the relatively cooler core fluid near the center of the channel. This mixing also serves to increase the heat transfer from the channel wall.

It has been shown that the ideal spacing for orthogonal ribs is approximately $P/e = 10$. As conceptually shown in Fig. 6a, with a $P/e = 10$ spacing, sufficient space is given between the ribs for reattachment of the flow between the ribs. However, as the ribs continue to move closer together, the reattachment area becomes jeopardized. After separation, the flow may impinge on the next downstream rib ($P/e = 5$) or the flow may completely pass over the next rib ($P/e = 2.5$), completely eliminating the desired flow behavior.

Ribs skewed to the mainstream flow are preferred to orthogonal ribs because they induce an angled secondary flow. The fluid near the surface follows the angle of the rib. This angled-rib-induced secondary flow creates a set of counter-rotating vortices in the channel. The secondary flow follows the rib until it impinges on the side wall, as shown in Fig. 6b. After impingement on the side wall, the secondary rib-induced flow returns to the other side wall, creating a vortex. This behavior is identical on both the leading and trailing surfaces, and so two counter-rotating vortices form in the channel. Rib-induced secondary flow obviously has a great impact on the heat transfer in the channel. Therefore, it is critical to optimize the rib configuration to take advantage of the rib-induced secondary flow. For instance, placing the rib at an angle so that it is not orthogonal to the mainstream flow significantly increases the heat transfer coefficients.

Because the ribs are skewed to the mainstream flow, regardless of how closely the ribs are spaced, the angled-rib-induced secondary flow is expected to be present, as shown in Fig. 6b. Unlike with 90 deg ribs, the fluid that is trapped between closely spaced angled ribs is expected to travel along the length of the ribs and create the counter-rotating vortices. Predictions from Su et al. [14] for a nonrotating channel with angled ribs ($P/e = 10$) show that the angled-rib-induced counter-rotating vortices are not limited to areas close to the rib-roughened walls; each vortex occupies nearly half of the channel cross section. If this trend is present, regardless of the rib spacing, the coolant between the ribs is moving (as opposed to being trapped), and additional heat transfer enhancement will occur.

The level of heat transfer enhancement in the two-pass channel with angled ribs is altered by the sharp 180 deg turn that connects the first pass to the second pass, by rotation, and by rotation-induced buoyancy forces. Figure 7 shows the secondary flows induced by angled ribs, the 180 deg turn, and rotation. The secondary flow induced by rotation is a result of the Coriolis force. As conceptually shown in Fig. 7a, with a 90 deg channel orientation, the Coriolis force

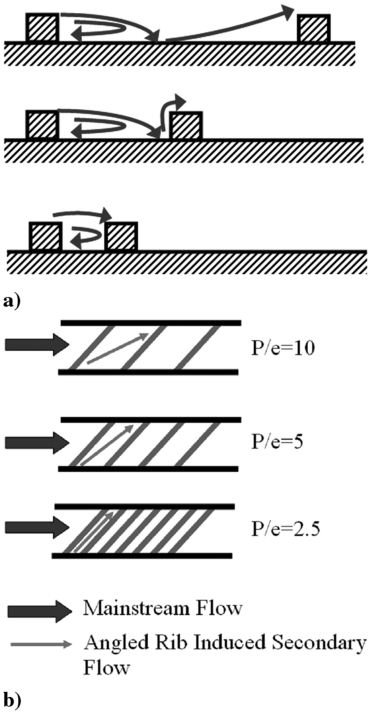

Fig. 6 Effects of rib spacing on a) mainstream flow separation and reattachment and b) angled-rib-induced secondary flow.

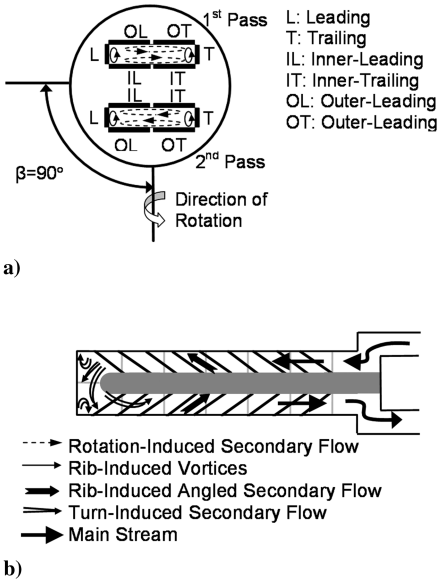

Fig. 7 Conceptual view of a) rib- and rotation-induced secondary flow inside a two-passage rectangular channel (AR = 1:4) and b) rib- and turn-induced secondary flow.

induces a pair of vortices that circulate toward the trailing wall for radially outward flow (first pass) and toward the leading wall for radially inward flow (second pass). This cross-stream secondary-flow pattern significantly increases heat transfer on the trailing wall in the first pass and the leading wall in the second pass. However, the rotation-induced secondary flow reduces heat transfer on the leading wall in the first pass and the trailing wall in the second pass. In the current study, the secondary flow caused by the 45 deg angled ribs that are located on the leading and trailing walls in the first pass causes impingement of the flow onto the outer wall. In the second pass, the secondary flow due to the ribs causes impingement onto the inner wall, as shown in Fig. 7a.

When the mainstream flow passes through the 180 deg turn, the flow impinges on the outer wall of the second pass, then reattaches on the inner wall in the second pass, as shown in Fig. 7b. A circulation zone right after the turn near the inner wall in the second pass is created due to the sharp turn. Two additional circulation zones occur in the outer corners of the turn because of the geometry. These flow structures due to the turn result in different heat transfer enhancements inside the turn and after the turn. All of these secondary flows (induced by angled ribs, the 180 deg turn, and rotation) interact to make flow through a rib-roughened serpentine passage very complex. The combination of these flows may result in further enhancement of the heat transfer or may have a negative impact on the heat transfer trend. The flow patterns previously described have been observed by previous studies (Han et al. [21], Han and Zhang [22], Ekkad and Han [23], Park and Lau [24], Park et al. [25], Liou et al. [26], and Liou and Chen [27]).

Rotation causes a difference in the heat transfer between the leading and trailing walls, as mentioned previously. The effect of rotation is evaluated by the rotation number Ro. The combined effect of rotation and temperature is evaluated by the local buoyancy parameter Bo_x. For the radially outward flow, the rotation-induced buoyancy force aids the inertial force. The rotation-induced buoyancy force opposes the inertial force in the second pass, because the flow direction reversed. A buoyancy parameter, as defined by Wagner et al. [7], is used to present the combined effects of the Coriolis and rotation-induced buoyancy forces:

$$Ro = (\Omega D_h)/U_b \tag{5}$$

$$Bo_x = \left(\frac{\Delta\rho}{\rho_{b,x}}\right)(Ro)^2\left(\frac{R_x}{D_h}\right) \tag{6}$$

This local buoyancy parameter can be rewritten by incorporating the measured wall and bulk air temperatures, as shown in Eq. (7):

$$Bo_x = \left(\frac{T_{w,x} - T_{b,x}}{T_{w,x}}\right)(Ro)^2\left(\frac{R_x}{D_h}\right) \tag{7}$$

In the current study, to more accurately determine the local buoyancy parameter, the local wall temperature in the denominator of Eq. (7) is replaced by the local film temperature $T_{f,x}$. The local film temperature is the average of the local wall and the local bulk temperatures, as shown in Eq. (8):

$$T_{f,x} = (T_{w,x} + T_{b,x})/2 \tag{8}$$

Stationary Results with Entrance Effects

All of the heat transfer results presented in the current study are based on the total area. A discussion on the effect of area in the determination of the Nu/Nu_o ratios is presented next. The entrance condition, whether fully developed or developing flow, has an effect on the heat transfer in the first pass. Figure 8 shows the stationary streamwise average of the leading and trailing Nu_s/Nu_o ratios for smooth and ribbed ($P/e = 10$) walls in the first pass. The different entrance conditions of fully developed and sharp bend are compared at Reynolds numbers of 10,000 and 40,000. For the current study ($P/e = 10$ sharp bend), at $Re = 10,000$, the Nu_s/Nu_o ratio is the highest when compared with all cases until $x/D_h = 3.125$, after which the $P/e = 10$ case with a fully developed entrance has the highest Nu_s/Nu_o ratio. At $Re = 40,000$, comparing the current study ($P/e = 10$ sharp bend) with the smooth-wall sharp-bend results of Liu et al. [18], it is seen that the effects of the ribs are not present in the first pass (both sets of data lie on top of each other).

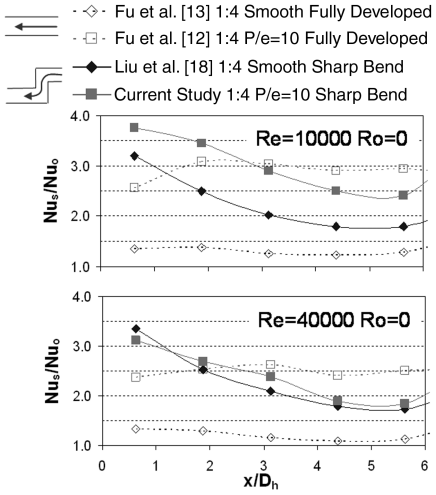

Fig. 8 Comparison of stationary streamwise-averaged Nu_s/Nu_o ratios with fully developed and sharp-bend entrance condition with smooth and ribbed ($P/e = 10$) walls in the first pass of the AR = 1:4 channel.

Channel-Averaged *Nu* Ratios with Area Effect

For a ribbed channel, when evaluating the heat transfer enhancement, the area used to perform the calculations can strongly impact the values of Nu/Nu_o ratios obtained. By adding ribs to the leading and trailing walls in the first pass and second pass, the total heat transfer area for the entire channel increases. In Table 1, the percent of area increase due to the ribs is shown for each P/e ratio tested. For the case of $P/e = 10$, the total area for the entire channel is only 1.28 times greater than for the smooth channel. However, for the case of $P/e = 2.5$, the total area for the ribbed channel is more than 2 times greater than for the smooth channel. Figure 9a shows the channel-averaged (leading and trailing) Nu_s/Nu_o ratios for the 1:4 AR test section under stationary conditions at the Reynolds numbers tested. For the smooth channel, the channel-averaged Nu_s/Nu_o ratio remains approximately constant for all Reynolds numbers at 2.0. For the ribbed cases, with the Nu_s/Nu_o ratio based on the total area, the Nu_s/Nu_o ratio increases with increasing P/e ratio. The $P/e = 10$ case shows the highest Nu_s/Nu_o ratios, based on the total area. However, for all ribbed cases, as the Reynolds number increases, the effect of the ribs decreases, and thus the Nu_s/Nu_o ratios decrease.

When the projected area is considered, the Nu_s/Nu_o ratios for the ribbed cases are higher when compared with the total area Nu_s/Nu_o ratios. For the 1:4 AR channel in this study, when the projected area is considered, the close rib spacing of the $P/e = 2.5$ case exhibits the highest heat transfer enhancement, although the $P/e = 5$ case is only slightly less. Liu et al. [15] showed a similar result. In their study (1:2AR), the close rib spacing of $P/e = 3$ showed the highest Nu_s/Nu_o ratios, based on the projected area. For the rotating case, as shown in Fig. 9b, similar trends are observed. It should be understood that when considering the rotating case, different rotation numbers are achieved at different Reynolds numbers, because the rotational speed is held constant at 400 rpm.

Table 1 Percentage of area increase due to ribs for the 3 P/e ratios tested for the entire channel

P/e	Area increase
10	27.89%
5	52.68%
2.5	105.37%

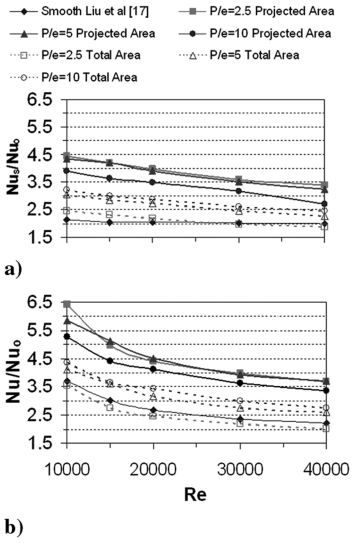

Fig. 9 Channel-averaged Nusselt number ratios as a function of Reynolds number: a) stationary and b) rotating (rpm = 400).

Rotating Results

Figures 10 shows the effect of increasing the rotational speed on the streamwise Nu/Nu_o ratio distribution for the leading and trailing surfaces, with smooth and ribbed walls at a Reynolds number of 10,000. From Fig. 10, the effect of rotation in a ribbed channel is visible when compared with the smooth case. For example, at $x/D_h = 3.125$ for all P/e ratios, between the rpm of 100 to 400, there are different values of Nu/Nu_o ranging from 1 to 3, whereas for the smooth case at the same location, Nu/Nu_o is about 2 for all rotational speeds. Also, note that for $P/e = 10$ (rpm = 0 to 200), the entrance effect is more prevalent, in that the Nu/Nu_o ratio continually decreases (for each rpm) until $x/D_h = 5.625$, and then an increase is experienced because of the turn. For the $P/e = 2.5$ and 5 cases, after $x/D_h = 3.125$ (rpm = 0 to 200), the Nu/Nu_o ratio remains approximately constant until $x/D_h = 5.625$, and then an increase is experienced because of the turn. For example, consider $P/e = 10$ (200 rpm): the Nu/Nu_o decreases from about 2 (at $x/D_h = 3.125$) to about 1 (at $x/D_h = 5.625$). For the $P/e = 2.5$ and 5 cases, at the same rpm and x/D_h range, the Nu/Nu_o ratio is constant at about 1. However, for an rpm value of 400, for all P/e ratios, the Nu/Nu_o ratio begins to increase after $x/D_h = 1.875$. This is similar to the smooth case of Liu et al. [18] and in a smooth square channel, as observed by Wagner et al. [7]. For all P/e ratios studied, note that in the first pass, as the rotational speed increases, the values of Nu/Nu_o fall below the stationary case. This is different from the smooth case, as observed by Liu et al. [18]. For all ribbed cases, on the leading surface for $x/D_h > 10$, the effect of rotation remains constant with increasing x/D_h, compared with the trailing surface. On the trailing surface for $x/D_h > 10$, as x/D_h increases, the effect of rotation decreases. This is observed by noting that the differences in Nu/Nu_o for different rotational speeds decrease in the streamwise direction on the trailing surface. Finally, for the second-pass trailing surface, at all P/e ratios, note that rotation increases the Nu/Nu_o ratios above the stationary case. This trend is different from that observed by Al-Hadhrami and Han [28] in a square channel.

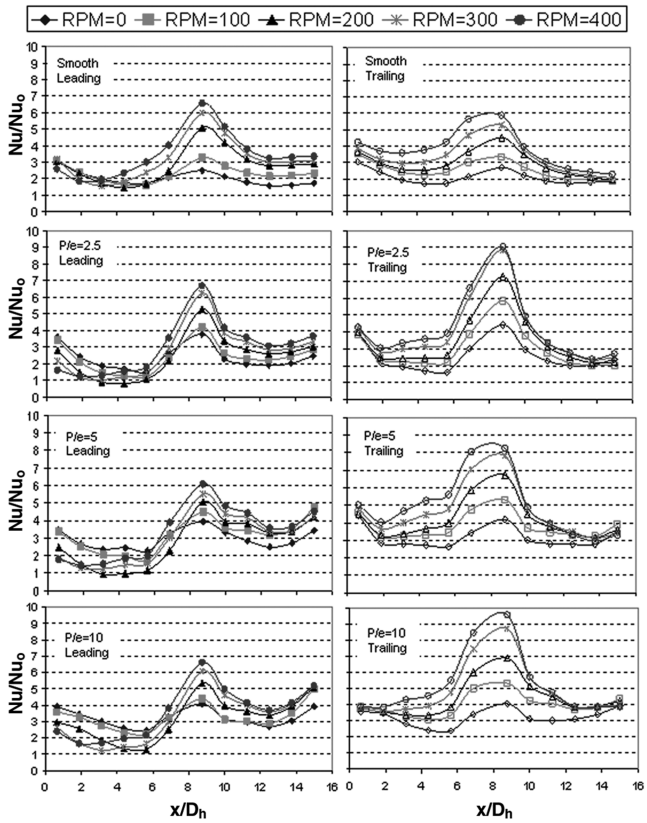

Fig. 10 Streamwise *Nu* ratio (Nu/Nu_o) distribution at $Re = 10,000$ for the leading and trailing walls.

Rotation Number Effects

The rotation number is a relative measure of the rotational Coriolis force and bulk flow inertia force (Han et al. [29]). In the current study, the rotation number is varied by the Reynolds number and the rotational speed. The rotation number in this study varied from 0 to 0.65. The data presented here are based on a wall temperature of 65°C and total area (3 times the rib-side area plus the smooth area between ribs). Figure 11 shows the Nu/Nu_s ratios as a function of Ro for the leading and trailing surfaces in regions 4 and 9. The stationary Nusselt number Nu_s is chosen as the denominator so that the effect of rotation on heat transfer can be compared.

In the first passage, the Coriolis forces push the core coolant toward the trailing surface. For all cases (ribbed and smooth) in region 4, the Nu/Nu_s ratio increases in a similar manner on the trailing surface as the rotation number increases. On the leading surface, for the smooth case, the Nu/Nu_s ratio decreases to a value of

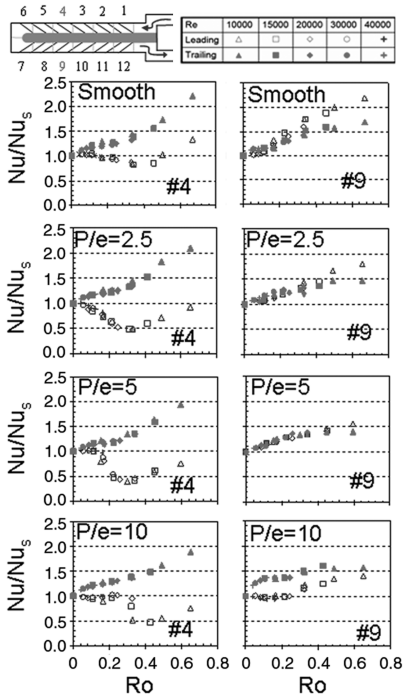

Fig. 11 Nu/Nu_s ratio distribution on the leading and trailing surfaces with respect to the rotation number in regions 4 and 9 for the smooth and all ribbed cases.

0.8 at a rotation number of 0.3. The Nu/Nu_s ratio then increases with the rotation number up to $Ro = 0.65$. However, for all ribbed cases, the Nu/Nu_s ratio decreases to a value of 0.5. The lower Nu/Nu_s ratio for the ribbed cases may be due to the reduced effect of the entrance condition when ribs are present. The increase of the Nu/Nu_s ratio on the leading surface after the critical Ro in all cases (ribbed and smooth) in region 4 is due to the development of large-scale reverse-flow cells, as reported by Wagner et al. [7] and Su et al. [14]. Also note that on the leading surface in region 4, as P/e increases, a decrease in the Nu/Nu_s ratios occurs at larger Ro values. This may imply that the effect of the entrance is reduced as the ribs are placed closer to each other.

In the second pass at region 9, the Coriolis forces push the core coolant toward the leading surface, because the flow is radially inward. Little difference is seen on the trailing surface between the smooth case and all ribbed cases. The trailing-surface heat transfer increases in a similar fashion for the smooth case and ribbed cases. The leading surface for the smooth case has the highest heat transfer enhancement due to rotation. As P/e increases, the effect of rotation on heat transfer on the leading surface in region 9 decreases. This shows that the heat transfer enhancement is dominated by the ribs rather than rotation.

Buoyancy-Parameter Effect

The buoyancy parameter Bo takes into account not only rotation, but the temperature difference between the heated wall and the cool mainstream flow. However, in this study, because only one density ratio based on inlet conditions is presented, the data are not an isolated buoyancy effect. Figures 12 and 13 show how the Nu/Nu_s ratio is affected by local Bo for all P/e ratios tested. Figure 12 shows regions 1, 4, and 6 and tip region 6, which are in the first pass. In region 1, for the smooth case and all ribbed cases, it is seen that the trailing-surface Nu/Nu_s ratio remains constant at 1 as Bo increases. This implies that the effects of the entrance dominate over rotation on the trailing surface in region 1, regardless if ribs are present. On the leading surface, the Nu/Nu_s ratio remains constant until a Bo value of 0.1, after which the Nu/Nu_s ratio begins to decrease to approximately 0.5. This trend is different from the smooth case, in which a decrease on the leading surface is not seen until a Bo of 1. Figure 12 also shows the effect of Bo at region 4. Region 4 is the location at which the effect of the entrance and the turn are the smallest in the first pass. The trailing-surface Nu/Nu_s ratios for all P/e ratios and the smooth case show similar trends. As Bo increases, the Nu/Nu_s ratios increase. On the leading surface, for $P/e = 2.5$, the Nu/Nu_s ratios show a decrease starting at a Bo of 0.02, whereas the $P/e = 5$ case shows a decrease on the leading-surface Nu/Nu_s ratios at a Bo of 0.1. The $P/e = 10$ case does not show a decrease until a Bo of 0.3. All P/e cases show that the leading-surface Nu/Nu_s ratios decrease until a critical Bo value is reached, after which the Nu/Nu_s ratios begin to increase. As mentioned previously, this is due to the development of large-scale reverse-flow cells. This trend in the smooth channel was also observed by Liu et al. [18]. However, note that for none of the ribbed cases do the leading-surface Nu/Nu_s ratios increase above 1 at the highest Bo values, as is the case for the smooth channel. In region 6, the trailing-surface heat transfer is similar for the smooth case and ribbed cases. The leading-surface heat transfer enhancement for the smooth case is constant at 1 and then begins to increase. However, for the ribbed cases, the leading-surface heat transfer enhancement decreases to values of 0.6–0.8 and then increases.

In the first pass (tip region 6) and in the second pass (tip region 7) (Fig. 13), the flow is very turbulent, due to the sharp 180 deg turn. Direct impingement of the mainstream flow occurs on tip region 6. Heat transfer in this region is high, due to this impingement. In tip region 7, as the flow is directed into the second pass, the flow circulates and is very turbulent, which results in high heat transfer. No ribs were placed on the tip-region copper plates, only on the adjacent leading and trailing walls in the first and second passes. Thus, minimal difference is expected between the ribbed cases and smooth case.

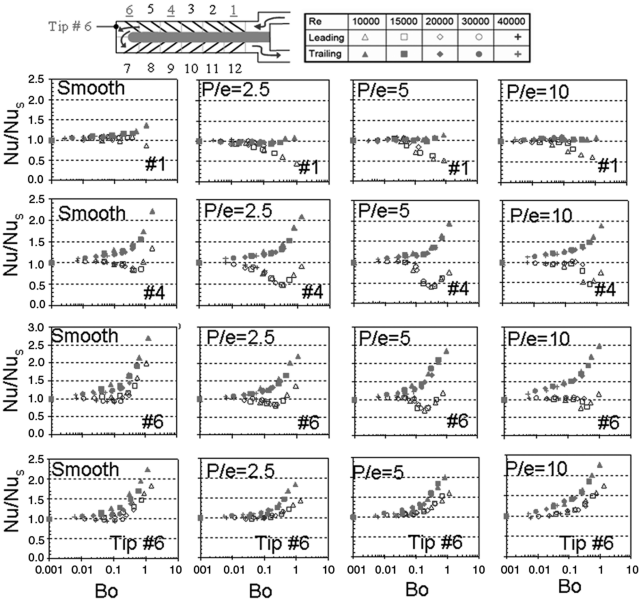

Fig. 12 Nu/Nu_s ratio distribution as a function of local buoyancy parameter in the first pass for smooth and ribbed cases.

In region 7, the heat transfer for the trailing surface and leading surface is similar for all ribbed cases. This may be due to the strong turbulence mixing that occurs as the flow changes direction around the turn. In region 9, as shown in Fig. 13, the Nu/Nu_s ratios on the trailing surface for all ribbed cases and smooth case are similar. The leading-surface Nu/Nu_s ratios increase with an increase in Bo for the smooth case. For all ribbed cases, the increase in Nu/Nu_s ratios due to rotation on the leading surface is less than for the smooth case in region 9. Figure 13 also shows the Nu/Nu_s ratios in region 12. The trailing-surface heat transfer for all cases is very similar. On the leading surface, there is little difference between Nu/Nu_s ratios of the ribbed cases. However, all ribbed cases show much lower Nu/Nu_s ratios than the smooth case on the leading surface in region 12. In region 12 for $P/e = 5$ and 10, the leading-surface heat transfer is always higher than the trailing-surface heat transfer. It

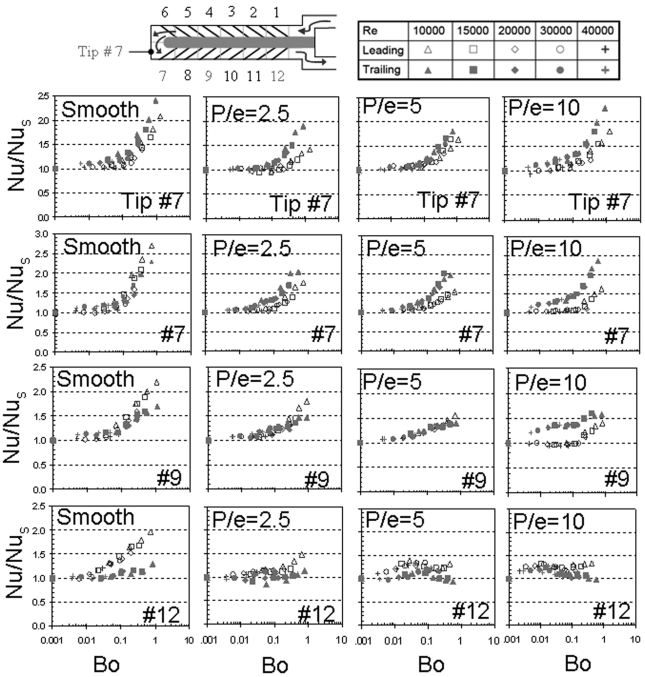

Fig. 13 Nu/Nu_s ratio distribution as a function of local buoyancy parameter in the second pass for smooth and ribbed cases.

appears that the data cross, but the data actually converge slightly and then diverge significantly.

Pass-Averaged Nu/Nu_s Ratios with Bo Correlations

Figure 14 presents the average Nu/Nu_s ratios on the leading and trailing surfaces in the first pass and second pass as a function of Bo for the smooth and ribbed cases. The average Nu/Nu_s ratios are for the six copper plates on each surface (leading and trailing) in each pass (first and second). For the $P/e = 10$ case, the current study is compared with that of Fu et al. [12], which had a fully developed entrance condition. The strong entrance condition of the current study dominates over the effects of rotation, as shown on the leading-surface average Nu/Nu_s ratios for the $P/e = 10$ case. A decrease in Nu/Nu_s ratios is not observed until a Bo of 0.3 for the current study, whereas the fully developed case (Fu et al.) shows a decrease earlier at a Bo of 0.1. For the trailing surface, there is not much difference in Nu/Nu_s ratios between the fully developed case and the sharp-bend entrance for the $P/e = 10$ case. For the smooth case, a clear difference is seen on the trailing surface between the fully developed condition (Fu et al.) and the sharp-bend entrance condition. The second-pass-averaged Nu/Nu_s ratios for the smooth and ribbed cases are also shown in Fig. 14. Comparing the $P/e = 10$ case with that of Fu et al. shows that not much difference is seen. First, this shows that the entrance condition is not impacting the heat transfer in the second pass. Second, the data from the current study are reliable, because the $P/e = 10$ data for the current study agree with that of Fu et al. The data should agree, because the same sharp 180 deg turn is present in both studies.

The data in the current study have been correlated using a power-law function, as shown in Eq. (9):

$$Nu/Nu_s = A \cdot Bo^a + B \cdot Bo^b + C \cdot Bo^c + D \tag{9}$$

There is a discrepancy of $\pm 10\%$ for $P/e = 2.5$ and $\pm 7\%$ for $P/e = 5$ between the experimental data and the correlation. For the $P/e = 10$ case, the correlation for the leading surface in the first pass has a discrepancy of $\pm 17\%$. However, the trailing surface in the first pass and both the leading and trailing surfaces in the second pass correlate very well and are within $\pm 9\%$. In Table 2, the coefficients and exponents that correspond to Eq. (9) are shown for the smooth case and ribbed cases.

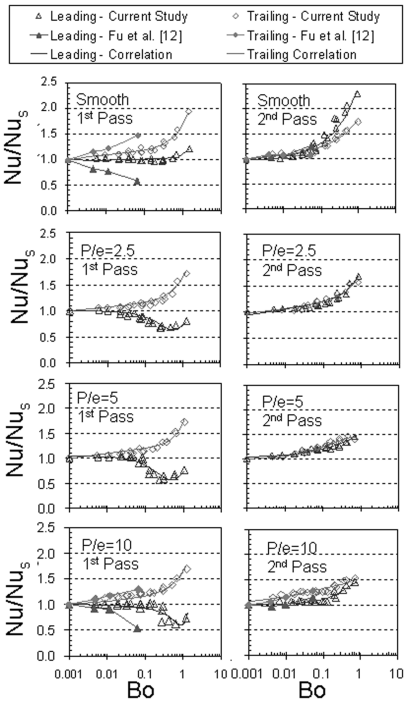

Fig. 14 Average Nu/Nu_s ratios (6 points) on the leading and trailing walls in the first and second passes for smooth and ribbed cases.

Table 2 Coefficients and exponents for Nu/Nu_s correlations[a]

	T2	T1	L2	L1
		Smooth		
A	1.21	1.23	1.20	1.04
B	0.57	0.44	1.25	0.19
C	0.00	0.00	0.00	0.00
D	0.00	0.00	0.00	0.00
a	0.03	0.03	0.04	0.01
b	0.69	1.20	0.75	5.60
c	0.00	0.00	0.00	0.00
		$P/e = 2.5$		
A	1.29	1.30	1.33	−1.75
B	0.50	0.48	0.50	3.48
C	0.00	−0.19	0.00	−2.00
D	0.00	0.06	0.00	1.00
a	0.04	0.04	0.05	2.69
b	1.20	1.10	1.30	2.09
c	0.00	0.21	0.00	1.14
		$P/e = 5$		
A	1.55	1.37	1.10	−2.21
B	−0.15	0.47	0.40	4.58
C	0.11	−0.20	0.14	−2.70
D	−0.07	0.09	−0.11	1.05
a	0.13	0.06	0.04	2.71
b	2.00	1.60	0.49	1.99
c	−0.20	0.30	−0.11	1.06
		$P/e = 10$		
A	3.30	1.30	−1.60	1.42
B	−5.00	0.48	1.51	−1.55
C	2.34	−0.19	0.52	−0.25
D	1.00	0.06	1.00	1.00
a	1.15	0.04	2.10	2.80
b	0.90	1.10	1.85	2.30
c	0.51	0.21	0.70	0.60

[a]T denotes trailing, L denotes leading, 1 denotes the first pass, and 2 denotes the second pass.

Conclusions

This study experimentally investigated the heat transfer in a rotating (90 deg orientation), two-pass, 1:4 AR channel with parallel ribs on the leading and trailing surfaces in the first pass and second pass. The rib angle was held constant at 45 deg. Square ribs with a height e of 1.59 mm were used and the e/D_h ratio was 0.078. The exhaustive testing matrix consisted of three P/e ratios: $P/e = 2.5, 5$, and 10. For each P/e ratio, the Reynolds numbers tested were 10,000, 15,000, 20,000, 30,000, and 40,000. For each Reynolds number, five rotational speeds were considered: 0, 100, 200, 300, and 400 rpm. The test section had a sharp-bend entrance, and thus the flow at the test-section entrance was not fully developed. Comparisons have been made with a smooth-case 1:4 AR channel with a fully developed entrance and a sharp-bend entrance. From the research work performed in this study, the following observations and conclusions were made:

1) For the stationary case, the channel-averaged Nu_s/Nu_o ratio is highest for the $P/e = 2.5$ case, based on the projected area. When the channel-averaged Nu_s/Nu_o ratio is based on the total area, the $P/e = 10$ case has the highest Nu_s/Nu_o ratios.

2) The effect of the sharp-bend entrance dominates over the rotation effects on the trailing surface, regardless of whether the wall is ribbed or smooth near the entrance. However, for the leading surface, for all P/e ratios, the effects of rotation dominate over the entrance condition when Bo is greater than 0.1.

3) The heat transfer for all P/e ratios and the smooth case on the trailing wall in the first pass increase with an increase of Ro. For the ribbed cases, the leading surface in the first pass initially shows a decrease in Nu/Nu_s ratios to a value of 0.5 until a critical Ro value of 0.3 is reached. Afterward, the heat transfer begins to increase on the leading surface.

4) In the second pass, the trailing-surface and leading-surface Nu/Nu_s ratios only increase slightly with Ro for all P/e ratios.

5) In the tip portion, the Nu/Nu_s ratios increase with Ro and Bo. Little difference is seen between the smooth case and all ribbed cases.

6) The rotation number and buoyancy parameter have been extended to values of 0.65 and 1.5, respectively. Bo correlations developed in this study show that the buoyancy parameter can be used in the higher range to satisfactory levels of accuracy to predict the effects of rotation (Nu/Nu_s).

Acknowledgment

This work has been funded through the Marcus Easterling Endowment Fund.

References

[1] Han, J. C., "Heat Transfer and Friction Characteristics in Rectangular Channels with Rib Turbulators," *Journal of Heat Transfer*, Vol. 110, No. 2, 1988, pp. 321–328.

[2] Han, J. C., and Park, J. S., "Developing Heat Transfer in Rectangular Channels with Rib Turbulators," *International Journal of Heat and Mass Transfer*, Vol. 31, No. 1, 1988, pp. 183–195. doi:10.1016/0017-9310(88)90235-9

[3] Park, J. S., Han, J. C., Huang, Y., and Ou, S., "Heat Transfer Performance Comparisons of Five Different Rectangular Channels with Parallel Angled Ribs," *International Journal of Heat and Mass Transfer*, Vol. 35, No. 11, 1992, pp. 2891–2903. doi:10.1016/0017-9310(92)90309-G

[4] Taslim, M. E., and Spring, S. D., "Effects of Turbulator Profile and Spacing on Heat Transfer and Friction in a Channel," *Journal of Thermophysics and Heat Transfer*, Vol. 8, No. 3, 1994, pp. 555–562. doi:10.2514/3.578

[5] Han, J. C., Glicksman, L. R., and Rohsenow, W. M., "An Investigation of Heat Transfer and Friction for Rib-Roughened Surfaces," *International Journal of Heat and Mass Transfer*, Vol. 21, No. 8, 1978, pp. 1143–1156. doi:10.1016/0017-9310(78)90113-8

[6] Han, J. C., "Heat Transfer and Friction in Channels with Two Opposite Rib-Roughened Walls," *Journal of Heat Transfer*, Vol. 106, No. 4, 1984, pp. 774–781.

[7] Wagner, J. H., Johnson, B. V., and Hajek, T. J., "Heat Transfer in Rotating Passages with Smooth Walls and Radial Outward Flow," *Journal of Turbomachinery*, Vol. 113, No. 1, 1991, pp. 42–51. doi:10.1115/1.2927736

[8] Wagner, J. H., Johnson, B. V., and Kooper, F. C., "Heat Transfer in Rotating Passage with Smooth Walls," *Journal of Turbomachinery*, Vol. 113, No. 3, 1991, pp. 321–330. doi:10.1115/1.2927879

[9] Taslim, M. E., Bondi, L. A., and Kercher, D. M., "An Experimental Investigation of Heat Transfer in an Orthogonally Rotating Channel Roughened with 45 Deg Criss-Cross Ribs on Two Opposite Walls," *Journal of Turbomachinery*, Vol. 113, No. 3, 1991, pp. 346–353. doi:10.1115/1.2927882

[10] Azad, G. S., Han, J. C., Moon, H. K., and Glezer, B., "Heat Transfer in a Two-Pass Rectangular Rotating Channel with 45-Deg Angled Rib Turbulators," *Journal of Turbomachinery*, Vol. 124, No. 2, 2002, pp. 251–259. doi:10.1115/1.1450569

[11] Al-Hadhrami, L. M., Griffith, T. S., and Han, J. C., "Heat Transfer in Two-Pass Rotating Rectangular Channels ($AR = 2$) with Parallel and Crossed 45° V-Shaped Rib Turbulators," AIAA Paper 2002-0789, 2002.

[12] Fu, W. L., Wright, L. M., and Han, J. C., "Heat Transfer in Two-Pass Rotating Rectangular Channels ($AR = 1{:}2$ and $AR = 1{:}4$) with 45° Angled Rib Turbulators," American Society of Mechanical Engineers Paper GT 2004-53261, 2004.

[13] Fu, W. L., Wright, L. M., and Han, J. C., "Buoyancy Effects on Heat Transfer in Five Different Aspect-Ratio Rectangular Channel with Smooth Walls and 45-Degree Ribbed Walls," American Society of Mechanical Engineers Paper GT 2005-68493, 2005.

[14] Su, G., Chen, H. C., Han, J. C., and Heidmann, D.,"Computation of Flow and Heat Transfer in Two-Pass Rotating Rectangular Channels ($AR = 1{:}1$, $AR = 1{:}2$, $AR = 1{:}4$) with 45-Deg Angled Ribs by a Reynolds Stress Turbulence Model," American Society of Mechanical Engineers Paper GT2004-53662, 2004.

[15] Liu, Y. H., Wright, L. M., Fu, W. L., and Han, J. C., "Rib Spacing Effect on Heat Transfer and Pressure Loss in a Rotating Two-Pass Rectangular Channel ($AR = 1{:}2$) with 45-Degree Angled Ribs," American Society of Mechanical Engineers Paper GT2006-90368, 2006.

[16] Wright, L. M., Fu, W. L., and Han, J. C., "Influence of Entrance Geometry on Heat Transfer in Rotating Rectangular Cooling Channels ($AR = 4{:}1$) with Angled Ribs," *Journal of Heat Transfer*, Vol. 127, No. 4, 2005, pp. 378–387. doi:10.1115/1.1860564

[17] Wright, L. M., Liu, Y. H., Han, J. C., and Chopra, S., "Heat Transfer in Trailing Edge, Wedge-Shaped Cooling Channels under High Rotation Numbers," American Society of Mechanical Engineers Paper GT2007-27093, 2007.

[18] Liu, Y. H., Huh, M., Han, J. C., and Chopra, S., "Heat Transfer in a Two-Pass Rectangular Channel (1:4) Under High Rotation Numbers," American Society of Mechanical Engineers Paper GT2007-27067, 2007.

[19] Kays, W., Crawford, M., and Weigand, B., *Convection Heat and Mass Transfer*, McGraw–Hill, New York, 2005.

[20] Kline, S. J., and McClintock, F. A., "Describing Uncertainty in Single-Simple Experiments," *Mechanical Engineering*, Vol. 75, Jan. 1953, pp. 3–8.

[21] Han, J. C., Chandra, P. R., and Lau, S. C., "Local Heat/Mass Transfer Distributions Around Sharp 180 Deg. Turns in Two-Pass Smooth and Rib-Roughened Channels," *Journal of Heat Transfer*, Vol. 110, No. 1, 1988, pp. 91–98.

[22] Han, J. C., and Zhang, P., "Effect of Rib-Angle Orientation on Local Mass Transfer Distribution in a Three-Pass Rib Roughened Channel," *Journal of Turbomachinery*, Vol. 113, No. 1, 1991, pp. 123–130. doi:10.1115/1.2927730

[23] Ekkad, S. V., and Han, J. C., "Detailed Heat Transfer Distribution in Two-Pass Square Channels with Rib Turbulators," *International Journal of Heat and Mass Transfer*, Vol. 40, No. 11, 1997, pp. 2525–2537. doi:10.1016/S0017-9310(96)00318-3

[24] Park, C. W., and Lau, S. C., "Effect of Channel Orientation of Local Heat (Mass) Distributions in a Rotating Two-Pass Square Channel with Smooth Walls," *Journal of Heat Transfer*, Vol. 120, No. 3, 1998, pp. 624–632. doi:10.1115/1.2824323

[25] Park, C. W., Yoon, C., and Lau, S. C., "Heat (Mass) Transfer in a Diagonally Oriented Rotating Two-Pass Channel with Rib-Roughened Walls," *Journal of Heat Transfer*, Vol. 122, No. 1, 2000, pp. 208–211. doi:10.1115/1.521460

[26] Liou, T. M., Tzeng, Y. Y., and Chen, C. C., "Fluid Flow in a 180 Deg Sharp Turning Duct with Different Divider Thicknesses," *Journal of Turbomachinery*, Vol. 121, July 1999, pp. 569–575.

[27] Liou, T. M., and Chen, C. C., "LDV Study of Developing Flows Through a Smooth Duct with a 180 Deg Straight-Corner Turn," *Journal of Turbomachinery*, Vol. 121, Jan. 1999, pp. 167–174.

[28] Al-Hadhrami, L., and Han, J. C., "Effect of Rotation on Heat Transfer in Two-Pass Square Channels with Five Different Orientations of 45° Angled Rib Turbulators," *International Journal of Heat and Mass Transfer*, Vol. 46, Feb. 2003, pp. 635–669.

[29] Han, J. C., Dutta, S., Ekkad, S. V., *Gas Turbine Heat Transfer and Cooling Technology*, Taylor and Francis, New York, 2000.